Int. J. Electrochem. Sci., 13 **(2018)** 6565 – 6576, doi: 10.20964/2018.07.62

International Journal of
ELECTROCHEMICAL
SCIENCE
www.electrochemsci.org

Synthesis and Electrochemical Properties of Flower-like Na-doped V_6O_{13} Cathode Materials for Li-ion Batteries

Zhendong Wan, Zhengguang Zou[*]*, Jilin Wang, Fei Long, Yi Wu*

Ministry-province Jointly-constructed Cultivation Base for State Key Laboratory of Processing for Non-ferrous Metal and Featured Materials, Guilin University of Technology, Guilin, China.
[*]E-mail: zouzgglut@163.com

Received: 9 March 2018 / *Accepted:* 2 May 2018 / *Published:* 5 June 2018

Flower-like $Na_xV_6O_{13}$ samples (x=0~0.535) are fabricated via a typical hydrothermal method followed by annealed process at 350°C for 1h in argon atmosphere. The phase structure, chemical composition, morphology and element valence of prepared samples are characterized by XRD, XPS, FESEM and EDS. The electrochemical properties of prepared samples are measured by CV, EIS and charge-discharge analyses. These results demonstrates that the enhancement of electrochemical reversibility in Na-doped V_6O_{13} cathode materials are attributed to its high total conductivity, low charge transfer resistance and better electrochemical reversibility. In addition, both crystal domain size and the lithium diffusion coefficient of the Na-doped V_6O_{13} samples are influenced by the added amount of $NaNO_3$. When the doped molar ratio of Na^+ to V_6O_{13} is 0.321/1, the product presents hierarchical flower-like microsphere morphologies, which is assembled by interconnected nanorods. It demonstrates the best electrochemical performance with initial discharge capacity of 422.47mA·h/g. After 100cycles, the discharge capacity and capacity retention of $Na_{0.321}V_6O_{13}$ are 215.30mA·h/g and 51% respectively.

Keywords: Cathode Materials; Li-ion Batteries; V_6O_{13}; Na-doping

1. INTRODUCTION

Continuous development of large-scale storage applications is highly demanded for energy storage technologies. In particular, the high-performance lithium-ion batteries (LIBs) is one of the most promising battery technologies [1-3]. As for the ideal LIBs, it possesses excellent electrochemical performance, and the cathode materials plays a significant role in terms of electrochemical performance. And the corresponding battery electrode materials should simultaneously provide high-energy density, high-rate capability and low self-discharge energy density [4].

The previous researches have reported various typical cathode materials [5-8], such as $LiCoO_2$, $LiNiO_2$, $LiMnO_2$, $LiFePO_4$, etc. More importantly, these materials have made great success in commercialization [9, 10]. However, fabrication of the ideal electrodes still face with great challenges,

and cathode materials still limit the further development of the rechargeable LIBs [11, 12]. For example, rechargeable LIBs assembled from these cathode materials possess low discharge capacity (less than 150mA·h/g) due to their low theoretical specific capacity.

Recently, vanadium oxide-based materials has been founded to be a kind of promising candidate in the cathode materials of rechargeable LIBs due to stable layer structure, multiple vanadium oxidation states, high specific capacity and widely availability [13-15]. A variety of vanadium oxide-based materials [16] have been synthesized in previous literatures, including V_2O_5, V_6O_{13}, V_3O_7, VO_2, and so on. Among these vanadium oxide-based materials, V_6O_{13} has attracted attention on account of its high rate capability, good reversible capacity, small volume expansion, low cost and safe lithiation potential. The theoretical specific capacity of V_6O_{13} reaches up to 420mA·h/g [17, 18] and 8mol lithium ions can be embedded in the internal structure of 1mol V_6O_{13}. However, it is difficult to prepare V_6O_{13} owing to valence fluctuation of vanadium in V_6O_{13} between +4 and +5. In addition, poor cycling performance, decayed discharge plateau and unsteady structure of V_6O_{13} have become serious obstacles when it is used as cathode materials of rechargeable LIBs [19]. In order to solve the problems mentioned above about V_6O_{13} cathode materials, an important approach to enhance the electrochemical properties of V_6O_{13} is via the substitution of vanadium-ion or vacancy with other cations.

It is confirmed that electrochemical performance of V_6O_{13} electrode materials has improved when Cations (such as Ag^+, Mn^{2+} and Ti^{4+}) are used as typical dopant in V_6O_{13}. As for doped ions, the doped position and reaction mechanism in the V_6O_{13} structure can be classified into three types [20]. The first kind of cations is Ag^+ or K^+, which can replace vacancies. The second cations is variable valence ions such as Mn^{2+} or Cr^{3+}, which can carry out replacement of V^{4+}/V^{5+}. The third cations is stable valence ion (Cu^{2+} or Ti^{4+}), which can also replace V^{4+}/V^{5+}. On the one hand, Na^+ and Li^+ are both first main group elements in the periodic table and display similar physicochemical property. Therefore, Na^+ can occupy the positon of lithium-ion vacancy and form $Li_xV_6O_{13}$ [21]. On the other hand, sodium is also one of the good conductive fillers, which can improve electrochemical performance of electrodes ($Na_{1+x}V_2O_5$ and $Na_{1+x}V_3O_8$) [22, 23]. However, it is rarely been reported about the effect of Na-ion doping on the structure and electrochemical performance of V_6O_{13}.

In this work, Na^+-doped V_6O_{13} are fabricated via a typical hydrothermal method followed by annealed process at 350°C for 1h in argon atmosphere. The phase structure, chemical composition, morphology and element valence of the as-prepared samples are characterized by XRD, XPS, FESEM and EDS. And the electrochemical properties are measured by CV, EIS and charge-discharge analyses. Finally, the comparative experiment is also performed to investigate the effect mechanism for the electrochemical performance of Na-doped V_6O_{13} electrode materials.

2. EXPERIMENTAL

2.1. Synthesis of Na doping V_6O_{13}

Na-doped V_6O_{13} compounds is synthesized by a typical hydrothermal method followed by heated at 350°C about 1h. All reagents are analytical grade with no need for any purification. In a typical procedure of synthesis, 1.25g of crystalline $C_2H_2O_4·2H_2O$ powder and 0.4g of crystalline V_2O_5

powder are dispersed in 20mL of ultrapure water. The mixtures are constantly stirred at 80°C for 5min. When the mixtures is cooled down to room temperature naturally, $(VO)(C_2O_4)$ solution is obtained after filtered.

After that, a certain amount of crystalline $NaNO_3$ powder (Table 1) is dissolved in 15mL of ultrapure water. Then 15mL $NaNO_3$ solution, 20mL $(VO)(C_2O_4)$ solution and 3mL H_2O_2 solution (30%) are transferred into a 100mL autoclave. And the autoclave is kept in an oven at 160°C for 24h. When the hydrothermal reaction is finished, the gained V_6O_{13} precursor is dried at -50°C for 24h. And the V_6O_{13} precursor is heated at rate of 3°C /min up to 350°C and kept for 1h in nitrogen atmosphere. Finally, the Na-doped V_6O_{13} samples are collected. The two main chemical reaction equations are as follows:

$$V_2O_5 + 3H_2C_2O_4 \cdot 2H_2O \rightarrow 2[(VO)(C_2O_4)] + 2CO_2\uparrow + 9H_2O$$

$$6(VO)(C_2O_4) + H_2O_2 + XNa^+ \rightarrow Na_xV_6O_{13} + H_2O + 12CO_2\uparrow$$

Table 1. Sample designations from doping different amount of crystalline $NaNO_3$ powder in V_6O_{13}

Sample designations	Sample proportion	$NaNO_3$/g
VO	V_6O_{13}	0
0.107VO	$Na_{0.107}$: V_6O_{13}	0.01
0.214VO	$Na_{0.214}$: V_6O_{13}	0.02
0.321VO	$Na_{0.321}$: V_6O_{13}	0.03
0.428VO	$Na_{0.428}$: V_6O_{13}	0.04
0.535VO	$Na_{0.535}$: V_6O_{13}	0.05

2.2. Characterization

X-ray diffraction (XRD) patterns are obtained on a Philips X'pert Pro diffractometer used *Cu*/*Kα* radiation source (λ=0.15406nm) at the scanned rate of 6°/min in the 2Θ range from 10 to 80°. X-ray photoelectron spectroscopy (XPS) analysis is carried out via an ESCALAB 250Xi spectrometer equipped with a multichannel detector. The spectra is excited by *Al*/*Kα* (1486.6eV) X-ray source of a twin anode and calibrated to the binding energy of the *C 1s* peak at 284.8eV in the constant analyzer energy mode with a base pressure of 10^{-8}Pa. The images of Field emission scanning electron microscopy (FESEM) are photographed by Hitachi S-4800 field emission scanning electron microscopy. Energy dispersive spectrometer (EDS, INCA IE 350 Oxford Instruments) is used to analyze component of the samples.

2.3. Electrochemical tests

In order to prepare the working electrodes for the electrochemical measurements, two electrode coin-type cells (CR 2025) are assembled in a glove box protected by ultrahigh-purity argon. 70% $Na_xV_6O_{13}$, 20% acetylene black and 10% polyvinylidene (PVDF) are dispersed in a proper amount of N-methy1-2pyrrolidone (NMP) solvent fluoride, and the mixtures are coated on Al foil. The cathodes

are obtained after Al foil is dried at 90°C for 12h in a vacuum oven. The electrolyte is made up of 1mol/L $LiPF_6$ dispersed in diethyl carbonate (DEC), ethylene carbonate (EC) and dimethyl carbonate (DEC). (DEC/EC/DMC=2:2:1 in volume). The separator is Celgard2400 membrane and the reference electrodes/counter is commercial Lithium metal. Galvanostatic charge/discharge measurements are tested by NEWARE CT-3008 5V10mA-164 Battery Testing System (BTS) in the potential range of 4.0-1.5V versus Li/Li^+. Electrochemical impedance spectroscopy (EIS) and cyclic voltammetry (CV) are determined on a CHI760D electrochemical workstation (Shanghai, China).

3. RESULTS AND DISCUSSION

3.1 Structure and morphology analysis

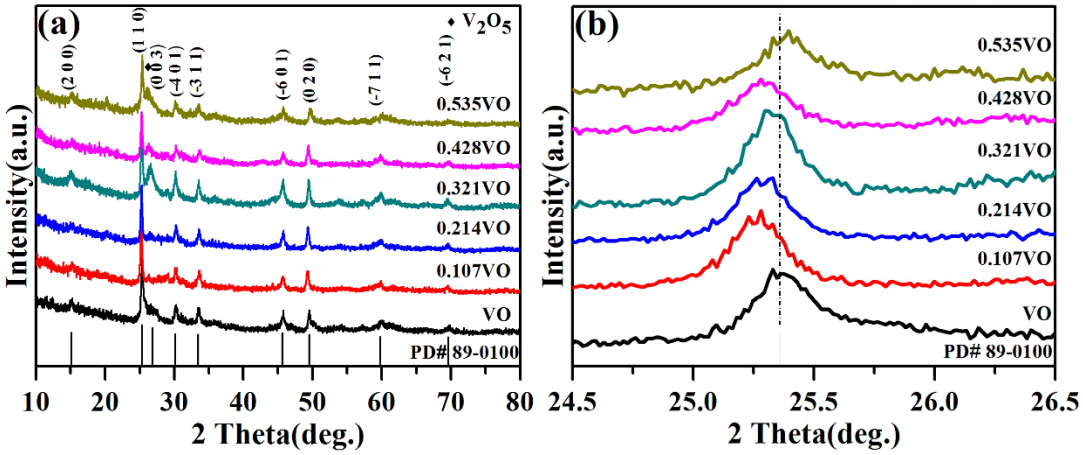

Figure 1. (a) XRD patterns of 0.107VO, 0.214VO, 0.321VO, 0.428VO and 0.535VO. (b) high angle patterns at 2 Theta degree ranging from 24.5° to 26.5° of 0.107VO, 0.214VO, 0.321VO, 0.428VO and 0.535VO.

Figure 1a shows that pure V_6O_{13} and Na-doped V_6O_{13} can be prepared with the help of low dose of $NaNO_3$ under this typical hydrothermal condition. While too much $NaNO_3$ (When the doped molar ratio of Na^+ to V_6O_{13} is 0.535/1) is added, the excessive $NaNO_3$ is reacted with $(VO)(C_2O_4)$ to form V_2O_5. Figure 1b shows the diffraction peaks shift to lower angle for all the Na-doped samples (except 0.535VO sample) when compared to that of the pure one. It means that ion doped can cause a slight change of lattice constant. The shift of diffraction peaks is ascribed to the dope of Na-ion because V (1.22Å) has the smaller covalent radius than that of Na (1.54Å). V-O covalent bond is weakened when Na^+ replaces the lithium-ion vacancy in $Li_xV_6O_{13}$ [21]. Lattice parameters and unit cell volumes for all samples are shown in Table 2. The unit cell volume of 0.321VO is 452$Å^3$, which is the largest in all samples. Volume expansion of unit cell indicates that Na^+ has incorporated into the Li^+ position of V_6O_{13} lattice. The variation of the lattice parameter in the Na-doped samples may be attributed to the combined effect of the ion-size misfit and the charge redistribution among Na^+, V^{4+} and V^{5+}.

Table 2. Lattice parameters and unit cell volume of V_6O_{13} with Na^+ doping

Sample designations	*a*(Å)	*b*(Å)	*c*(Å)	Volume (Å^3)
VO	11.2376	3.6185	10.0627	430
0.107VO	11.4242	3.6599	10.2135	437
0.214VO	11.6786	3.6897	10.5123	443
0.321VO	11.9407	3.7187	10.8374	452
0.428VO	11.8998	3.7089	10.7097	450
0.535VO	11.7356	3.7007	10.6097	447

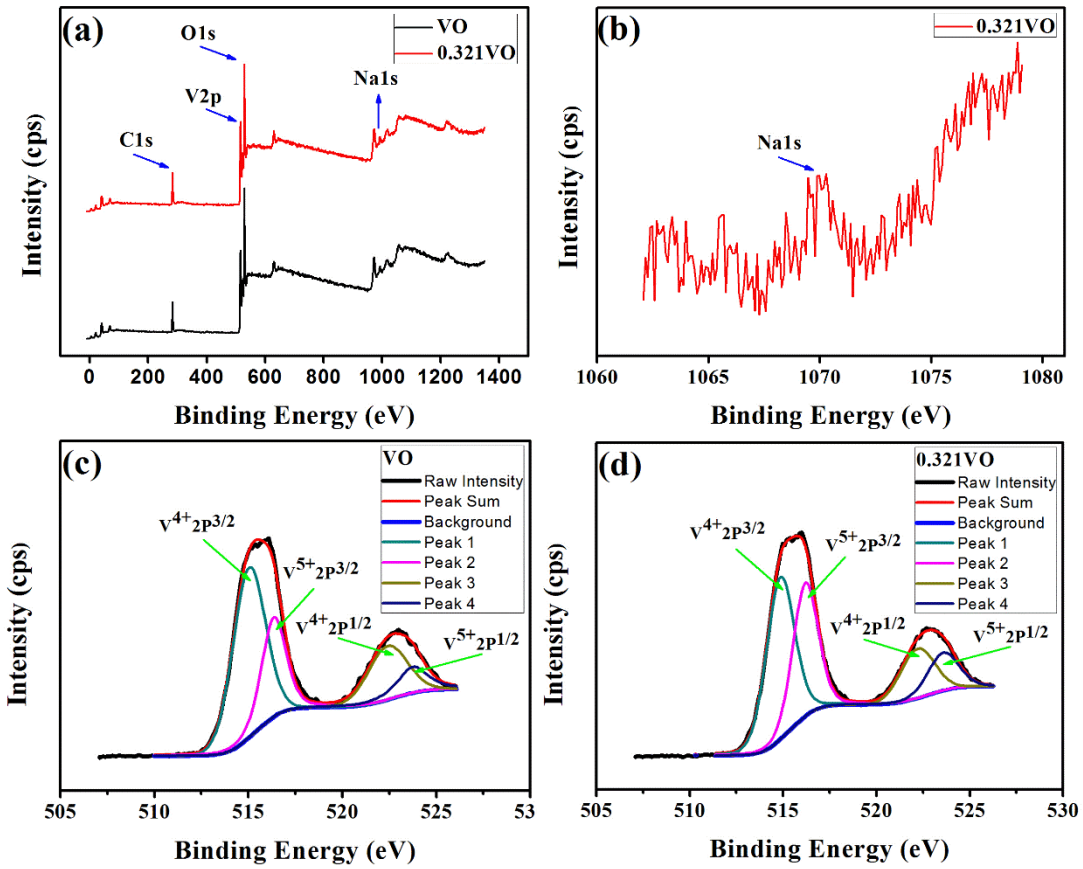

Figure 2. (a) XPS spectra of VO and 0.321VO. (b) Narrow-scan spectra in the *Na 1s* region of 0.321VO. (c) Narrow-scan spectra in the *V* $2P^{1/2}$ and *V* $2P^{3/2}$ region of VO. (d) Narrow-scan spectra in the *V* $2P^{1/2}$ and *V* $2P^{3/2}$ region of 0.321VO.

XPS spectra present the binding energy of the as-prepared samples VO and 0.321VO. As is shown in Figure 2c, the binding energy appears at 515.03eV, 516.34eV, 522.41eV and 523.73eV in VO, which are assigned to V^{4+} $2p_{3/2}$, V^{5+} $2p_{3/2}$, V^{4+} $2p_{1/2}$ and V^{5+} $2p_{1/2}$ peaks respectively. However, the corresponding binding energy are shifted to low values (514.85eV, 516.19eV, 522.20eV and 523.58eV) after Na-ions is doped in V_6O_{13} (Figure 2d). The molar ratio of V^{4+} and V^{5+} can be further calculated by means of the fitted curves. The related results are as follows, V^{4+} $2p_{3/2}$/V^{5+} $2p_{3/2}$ is 2.0/1

(VO) and 1.3/1 (0.321VO), $V^{4+}\ 2p_{1/2}/V^{5+}\ 2p_{1/2}$ is 2.0/1 (VO) and 1.3/1 (0.321VO) [19]. The proportion of V^{4+}/V^{5+} decreases and the binding energy shifts to low angle, indicating that Na-ion is successfully doped into the V_6O_{13} structure.

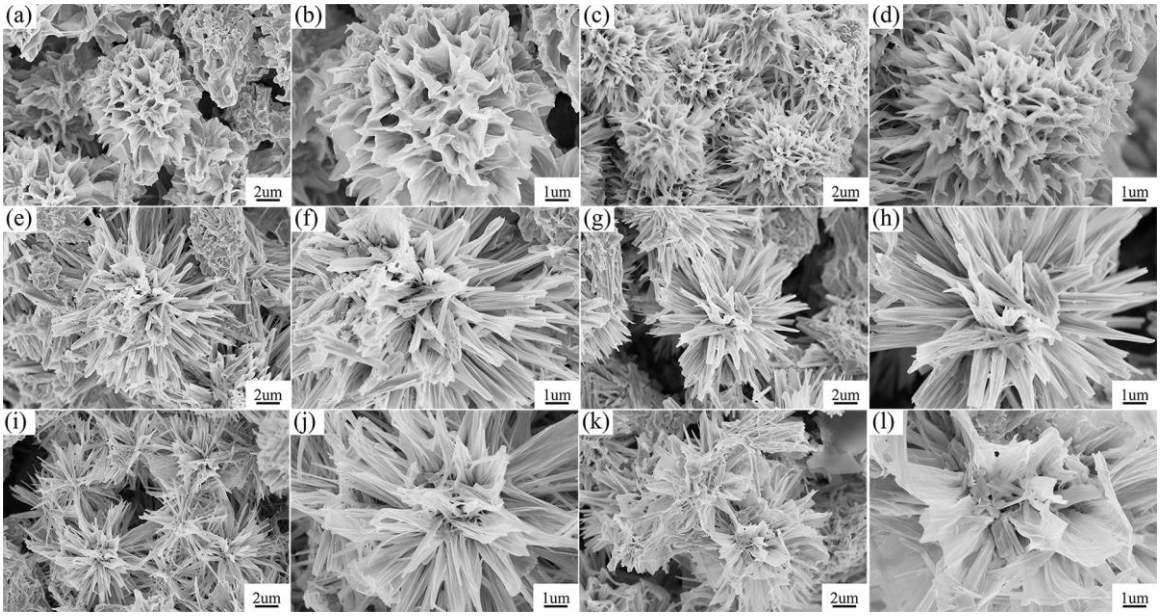

Figure 3. FESEM images of VO (a, b), 0.107VO (c, d), 0.214VO (e, f), 0.321VO (g, h), 0.428VO (i, j) and 0.535VO (k, l).

Figure 3 shows the FESEM images of Na-doped V_6O_{13} samples at different Na^+ contents. All samples demonstrate hierarchical flower-like microsphere morphologies, which are assembled from connected nanosheets. Plenty of structural voids are distributed in the surrounding area of the primary building blocks. The flower-like morphologies reveal larger special surface area in favor of lithium transport in the charge-discharge process. The lateral size of the nanosheets decreases with the increasing amount of doped Na-ions. However, superfluous Na-ions can lead to partial fracture structures. In addition, as the amount of Na-doped increases, the Na/V mole ratios in the samples also increase (Table 3).

Table 3. The theoretical molar ratio and experimental molar ratio of sodium to vanadium in different quantities Na-doped V_6O_{13}.

Sample designations	The theoretical molar ratio of Na/V	The experimental molar ratio of Na/V
VO	-	-
0.107VO	1.783×10^{-2}	1.600×10^{-2}
0.214VO	3.566×10^{-2}	2.396×10^{-2}
0.321VO	5.349×10^{-2}	3.813×10^{-2}
0.428VO	7.132×10^{-2}	5.411×10^{-2}
0.535VO	8.915×10^{-2}	5.720×10^{-2}

3.2 Electrochemical properties

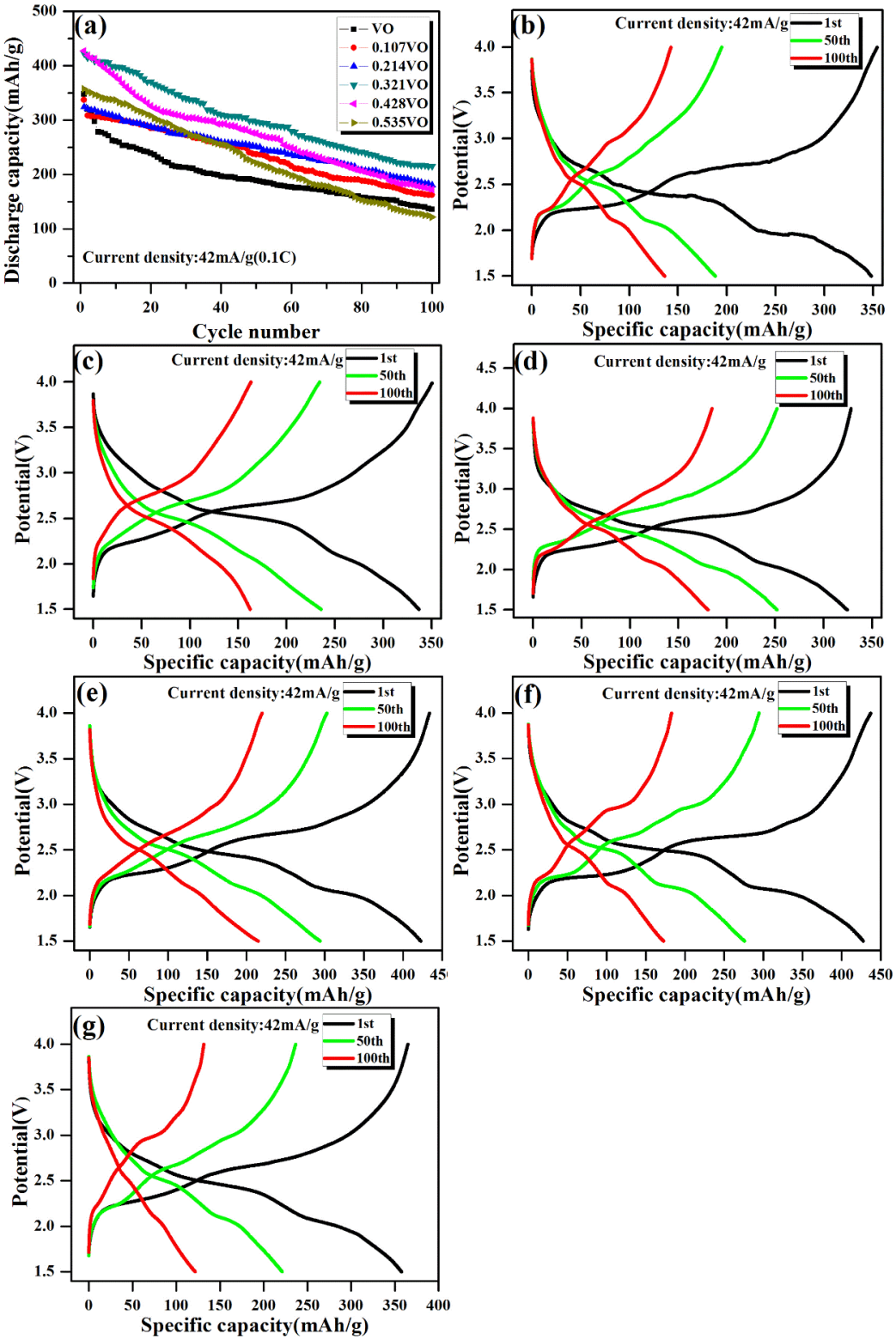

Figure 4. (a) Cyclic performance of electrodes fabricated in different Na-doped samples at 0.1C (42mA/g) discharge-charge rate. The 1st, 50th and 100th discharge/charge curves of VO (b), 0.107VO (c), 0.214VO (d), 0.321VO (e), 0.428VO (f) and 0.535VO (g) at current densities of 42mA/g in the voltage range of 1.5-4.0V.

Figure 4a presents the cycle performance of electrodes fabricated in different Na-doped samples at 0.1C (42mA/g) discharge-charge rate. It increases firstly and then decreases with increased doped contents of Na-ions. The discharge capacity in initial state and after 100 cycles continuously varies between 348.23mA·h/g and 136.15mA·h/g (VO), 337.12mA·h/g and 162.22mA·h/g (0.107VO), 324.45mA·h/g and 180.63mA·h/g (0.214VO2), 422.47mA·h/g and 215.30mA·h/g (0.321VO), 427.34mA·h/g and 172.63mA·h/g (0.428VO), 221.12mA·h/g and 121.59mA·h/g (0.535VO). The retention rates of capacities in sample VO, 0.107VO, 0.214VO, 0.321VO, 0.428VO and 0.535VO are 39%, 48%, 56%, 51%, 40% and 34% respectively. The sample 0.321VO displays the best cycle performance under comprehensive consideration for discharge/charge capacities and the retention rates of capacities. The wonderful cycle performance of 0.321VO is ascribed to its appropriate flower-like structure (Figure 3). The results of cycle performance show that the electrochemical performance of Na-doped V_6O_{13} is significantly better than that of the other similar cathode materials [24-31], which is presented in Table 4.

Table 4. The electrochemical performance of Na-doped V_6O_{13} and the other similar cathode materials.

Cathode materials	Initial discharge capacity (mA·h/g)	Capacity retention (%)	Cycle number
V_6O_{13} [24-26]	330	87	20
$K_{0.2}V_6O_{15.1}$[27]	378	60	15
$Ni_{1.0}V_6O_{15.9}$[27]	351	70	40
$Cr_{0.36}V_6O_{13.5}$[28, 29]	370	85	35
$Mn_xV_6O_{13}$ [30]	350	81	50
$V_6O_{12.3}$[31]	375	75	10
This work(0.321VO)	422	94/92/73	10/15/40

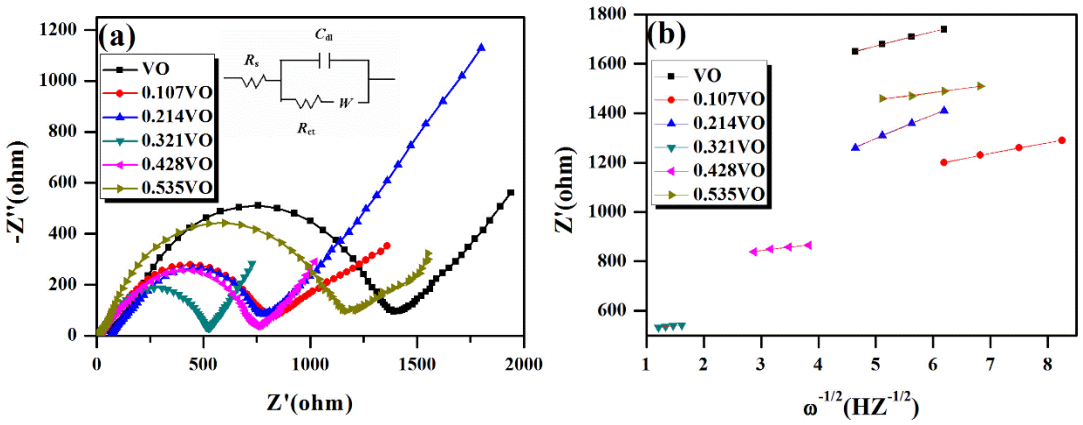

Figure 5. (a) Nyquist plots with equivalent circuit of 0.107VO, 0.214VO, 0.321VO, 0.428VO and 0.535VO. (b) Z' vs. $\omega^{-1/2}$ plots in the low-frequency region obtained from EIS measurements of 0.107VO, 0.214VO, 0.321VO, 0.428VO and 0.535VO.

Figure 4b-4g denotes 1st, 50th, and 100th charge-discharge curves of six samples at 0.1C (42mA/g). The voltage range is 1.5-4V at 25°C. Two distinct charge/discharge platforms appear near

2.3V and 2.7V. It means that the phase transition process happens in cathode material after intercalation and removal of lithium ions [32, 33]. However, the difference of charge platform in all samples is not very obvious. In order to study the true difference of electrochemical properties among all the samples, electrochemical impedance spectra (EIS) and cyclic voltammetry (CV) are further carried out.

EIS is measured at the 1th discharged state, and Figure 5a shows the Nyquist plots with equivalent circuit diagram. The diffusion coefficient of Li-ion (D_{Li}) in these samples can be evaluated from the plots at low frequencies by means of a numerical approximation, which is as follows [34, 35]:

$$D_{Li} = \frac{R^2T^2}{2A^2n^4F^4C^4{\sigma_w}^2}$$

R is the gas constant (8.314J·K^{-1}·mol^{-1}). T is the Kelvin temperature under measured (298.15K in this work). A is the surface area of the cathode (2cm^2 in this work). n is the number of electrons per molecule during cycling (obtained from initial discharge capacity). F is the Faraday constant (96485C/mol). C is the concentration of lithium ion (3.042×10^{-2}mol/cm^{-3} in this work). σ_w is the Warburg factor that can be obtained from the follow equation:

$$Z' = R_s + R_{ct} + \sigma_w \omega^{-1/2}$$

R_s is the resistance of the electrolyte and electrode material, R_{ct} is the charge transfer resistance, ω is the angular frequency in the range of low frequency [36, 37]. The relationship plot between Z' and $\omega^{-1/2}$ is shown in Figure 5b.

The EIS properties are summarized in Table 5, where the charge transfer resistance values vary greatly from each other. It is indicated that the amount of Na-doped has great effect on the charge transfer resistance. The R_{ct} value of the 0.321VO is the lowest in this work. It is adequately proved that the appropriate amount of Na-ions doped can make the electron transportation faster and the electrochemical polarization lower. With the doped amount of Na-ions increasing, the diffusion coefficient of Li^+ firstly increases and then decreases. The D_{Li} value of 0.321VO is the maximum value in this work, demonstrating that the appropriate doped amount of Na-ions not only can promote the ionic electronic conductivities but also shorten ionic diffusion path [38]. Therefore, the sample 0.321VO exhibits superior rate performance than that of the other samples in this work.

Table 5. Summary of the EIS properties of this work.

Sample designations	*Rs* (Ω)	*Rct* (Ω)	σ^w	D_{Li}(cm^2/s)
VO	30.11	1332	58.05866	0.281346×10^{-14}
0.107VO	14.42	723.4	43.72849	0.495958×10^{-14}
0.214VO	63.33	761.7	96.76444	0.101284×10^{-14}
0.321VO	12.18	508.4	22.24274	1.916891×10^{-14}
0.428VO	17.62	730.8	26.77562	1.322803×10^{-14}
0.535VO	10.61	1001	29.96143	1.056450×10^{-14}

The peak-positions of the anodic and cathodic potential change with the Na^+ doped content increase in this system (Figure 6). It is found that with the increase of doped content of Na-ion, the anodic peak first shifts to lower voltage and then shifts to higher voltage (0.214VO is the smallest). Instead, the cathodic peak first shifts to higher voltage then shifts to lower voltage (0.214VO is the largest). The cyclic voltammetry curves of 0.214VO have shown the largest polarization.

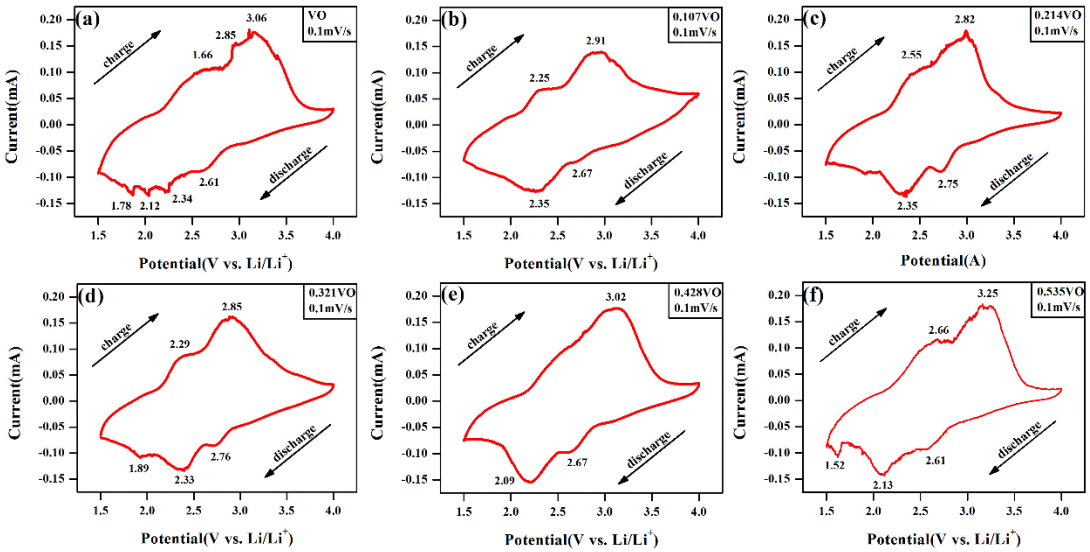

Figure 6. CV curves of VO (a), 0.107VO (b), 0.214VO (c), 0.321VO (d), 0.428VO (e) and 0.535VO (f) with the voltage range of 1.5-3.5V at the scanning speed of 0.1mV/s after charging/discharging 3 cycles.

Electrochemical reversibility [39] is obtained through the difference between anodic peak potential and corresponding cathodic peak potential. It proves that the smaller the ΔE_p value is, the better the electrochemical reversibility is. The equation for the calculation of ΔE_p by CV is expressed as follows:

$$\Delta E_p = E_{pa} - E_{pc}$$

E_{pa} is anodic peak potential, E_{pc} is cathodic peak potential. The ΔE_p of each sample are 0.94, 0.56, 0.47, 0.52, 0.93 and 1.12 V, which is corresponded to the retention rates of capacities in Figure 4a. The value of E_{pa} of sample 0.214VO is the smallest in all samples, which indicates good reversibility, excellent cyclability and high cyclic efficiency for lithium ion insertion/extraction at the electrodes [40].

4. CONCLUSION

Flower-like $Na_xV_6O_{13}$ samples (x~0-0.535) are fabricated via a typical hydrothermal method followed by annealed process at 350°C for 1h in argon atmosphere. Na-doped V_6O_{13} contains crystal domain size, electronic conductivity, initial discharge capacity, capacity retention and the diffusion

coefficient of Li^+, which are all influenced by the added amount of $NaNO_3$. In particular, when the doped molar ratio of Na^+ to V_6O_{13} is 0.321/1, the product demonstrates hierarchical flower-like microsphere morphologies, which are assembled in connected nanosheets. $Na_{0.321}V_6O_{13}$ exhibits the best electrochemical performance. The initial discharge capacity of 422.47mA·h/g is greater about 74.24mA·h/g than that of the sample with no doping. The capacity retention is 56% and is better than the pure sample (39%) after 100 cycles. The enhanced electrochemical performance originates from its low charge transfer resistance, high diffusion coefficient of lithium-ion, excellent electrochemical reversibility and better structure stability. These good performances suggest that flower-like Na-doped V_6O_{13} can be regarded as the potential cathode materials in lithium-ion batteries. We hope that this work can provide certain reference for the LIBs research and its application.

ACKNOWLEDGEMENTS
The authors gratefully acknowledge the National Nature Science Foundation of China (No.51562006)。

References

1. H. Price, E. Lupfert, D Kearney, E. Zarza, G. C. R. Gee and R. Mahoney, *Journal of Solar Energy Engineering*, 124 (2002) 109.
2. T. Ackermann and L. Soder, *Renewable and Sustainable Energy Reviews*, 4 (2000) 315.
3. V. R. Khramshin, S. A. Evdokimov, A. A. Nikolaev, A. A. Nikolaev, A. S. Karandaev, *Young Researchers in Electrical and Electronic Engineering Conference*, 4 (2015) 214.
4. P. Poizot, S. Laruelle, S. Grugeon, L. Dupont and J. M. Tarascon, *Nature*, 407 (2000) 496.
5. J. W. Fergus, *J. Power Sources*, 195 (2010) 939.
6. M. K. Song, S. J. Park, F. Alamgir, J. P. Cho and M. Liu, *Mat. Sci. Eng. R*, 72 (2011) 203.
7. K. T. Lee and J. Cho, *Nano Today*, 6 (2011) 28.
8. J. B. Goodenough and Y. Kim, *Chem. Mater.*, 22 (2010) 587.
9. B. Kang and G. Ceder, *Nature*, 458 (2009) 190.
10. M. Armand and J. M. Tarascon, *Nature*, 451 (2008) 652.
11. T. H. Kim, J. S. Park, S. K. Chang, S. D. Choi, J. H. Ryu and H. K. Song, *Adv. Energy Mater.*, 2 (2012) 860.
12. N. S. Choi, Z. H. Chen, S. A. Freunberger, X. L. Ji, Y. K. Sun, K. Amine, G. Yushin, L. F. Nazar, J. Cho and P. G. Bruce, *Angew. Chem. Int. Edit.*, 5 (2012) 19994.
13. J. Y. Song, Y. Y. Wang, C. C. Wan, *Journal of Power Sources*, 77 (1999) 183.
14. V. Etacheri, R. Marom, R. Elazari, G. Salitra and D. Aurbach, *Energy Environ. Sci.*, 4 (2011) 3243.
15. J. M. Tarascon and M. Armand, *Nature*, 414 (2001) 359.
16. J. Haber, M. Witko and R. Tokarz, *Appl. Catal. A-Gen.*, 157 (1997) 3.
17. N. Peys, Y. Ling, D. Dewulf, S. Gielis, C. D. Dobbelaere, D. Cuypers, P. Adriaensens, S. V. Doorslaer, S. D. Gendt, *Dalton Transactions*, 42 (2013) 959.
18. Y. Y. Xia, T. Fujieda, K. Tatsumi, P. P. Prosini and T. Sakai. Thermal, *Journal of Power Sources*, 92 (2001) 243.
19. Z. G. Zou, Q. Yuan, J. L. Wang, Y. Gao, Y. Wu, F. Long, S. C. Han, Z. D. Wan, *Int. J. Electrochem. Sci.*, 12 (2017) 1670.
20. J. Y. He, *Wuhan University of Technology*, 1 (2014) 1.
21. T. W. Graham, K. A. Udachin, *Chemical Communications*, 25 (2006) 2699.
22. T. Ohama, M. Isobe, Y. Ueda, *Physica B Physics of Condensed Matter*, 281 (2000) 650.
23. J. Kawakita, T. Miur, T. Kishi, *Solid State Ionics*, 224 (1999) 21.

24. Z. G. Zou, Z. L. Hou, J. L. Wang, Y. Gao, Z. D. Wan and S.C. Han, *Int. J. Electrochem. Sci.*, 12 (2017) 4979.
25. M. Sathiya, A. S. Prakash, K. Ramesha, J. M. Tarascon and A. K. Shukla, *Journal of the American Chemical Society*, 133 (2011) 16291.
26. S. N. Hua, S. Phang, *J Power Sources*, 10 (1983) 279.
27. M. Y. Saidi, J. Barker, *Solid State Ionics*, 78 (1995) 169.
28. P. Soudan, J. P. Pereira-Ramos, J. Farcy, G. Gregoire and N. Baffier, *Solid State Ionics*, 135 (2000) 291.
29. C. Leger, S. Bach, J. P. Pereira-Ramos, *J Solid State Electr*, 11 (2007) 71.
30. J. Y. He, F. Long, Z. G. Zou, *Ionics*, 21 (2015) 995.
31. Z. G. Zou, H. Chen, J. Y. He, F. Long, Y. Wu, Z. Y. Yan, H. X. Chen. *Electrochimica Acta*, 135 (2014) 175.
32. O. Bergstroem, T. Gustafsson and J. O. Thomas, *Acta Crystallogr. C*, 54 (1998) 1204.
33. J. Liu and A. Manthiram, *J. Phys. Chem. C*, 113 (2009) 15073.
34. J. Liu and A. Manthiram, *Chem. Mater.*, 21 (2009) 1695.
35. A. Y. Shenouda and H. K. Liu, *J. Power Sources*, 185 (2008) 1386.
36. A. Q. Pan, J. Liu, J. G. Zhang, G. Z. Cao, W. Xu, Z. M. Nie, X. Jie, D. Choi, B. W. Arey, C. M. Wang and S. Q. Liang, *J. Mater. Chem.*, 21 (2011) 1153.
37. Q. C. Zhuang, T. Wei, L. L. Du, Y. L. Cui, L. Fang and S. G. Sun, *J. Phys. Chem. C*, 114 (2010) 8614.
38. J. Y. He, W. M. Wang, Z. G. Zou, F. Long and Z. Y. Fu, *Ionics*, 20 (2014) 1063.
39. P. T. Kissinger and W. R. Heineman, *Journal of Chemical Education*, 60 (1983) 702.
40. L. C. Yang, Q. S. Gao, Y. Tang, Y. P. Wu, R. Holze, *J. Power Sources*, 185 (2008) 357.